Received: 4 December 2020 | Revised: 11 July 2021 | Accepted: 1 August 2021

DOI: 10.1111/ter.12555

RESEARCH ARTICLE

Terra Nova WILEY

Long distance plutonic relationships demonstrate 33 million years of strain partitioning along the Denali fault

Sean P. Regan[1,2] | Jeffrey A. Benowitz[2] | Trevor S. Waldien[3] | Mark E. Holland[4] | Sarah M. Roeske[3] | Paul O'Sullivan[5] | Paul Layer[2]

[1]Department of Geosciences, University of Alaska Fairbanks, Fairbanks, Alaska, USA

[2]Geophysical Institute, University of Alaska Fairbanks, Fairbanks, Alaska, USA

[3]Department of Earth and Planetary Sciences, University of California, Davis, California, USA

[4]Department of Life, Earth and Environmental Sciences, West Texas A&M University, Canyon, Texas, USA

[5]GeoSeps Services, Moscow, Idaho, USA

Correspondence
Sean P. Regan, Department of Geosciences, University of Alaska Fairbanks, 900 Yukon dr., Fairbanks, AK 99775, USA.
Email: sregan5@alaska.edu

Funding information
NSF EAR, Grant/Award Number: #1249885, #1828023, #0952834, #1828737 and #2120831; University of Alaska Fairbanks

Abstract

We identify two piercing point pairs along a ~500 km transect of the arcuate strike-slip Denali fault to document long-term slip partitioning. Geochemical and isotopic similarity between Foraker and Panorama-Schist Creek-Nenana Plutons suggest ~155 km of right-lateral displacement on the western Denali fault since 37 Ma at a rate of ~4.2 mm/year. The eastern Denali fault Maclaren-Cottonwood Terrane geochronology correlation establishes ~305 km of displacement on the eastern Denali fault since 33 Ma at a rate of ~9.2 mm/year. The ratio of Pleistocene-Holocene slip rates between the western (5.3 mm/year) and eastern (12.9 mm/year) Denali fault is 0.41 and our new constraints yield a Late Eocene-Holocene ratio of 0.46. Hence, we interpret that the overall arcuate geometry of the Denali fault master strand was established by 33 Ma. We infer that the persistent long-wave geometric stability of the Denali fault and other highly slip partitioned fault systems are related to long-term highly oblique transpressive environs.

1 | INTRODUCTION

Major strike-slip fault systems commonly display systematic variations in geodetic (Mahmoud et al., 2013; Tatar et al., 2012; Zheng et al., 2013) and Pleistocene-Holocene geologic slip rates (Liu et al., 2020; Matmon et al., 2006; Norris & Cooper, 2001; Zeng & Shen, 2014; Alchalbi et al., 2010, Kirby et al., 2007 exs. Altyn Tagh, Anatolia, Dead Sea, Denali, Kunlun, San Andreas). Decreasing strike slip-rate is generally attributed to strain partitioning whereby the missing slip is often taken up by dip-slip splay faults and distributed deformation off of the master strand of the fault (Burkett et al., 2016). Missing slip can also manifest as vertical tectonics proximal to the master strand as evidenced by high topography and/or rapid exhumation adjacent to strike-slip fault systems (Benowitz et al., 2011; Duvall et al., 2013; Spotila et al., 2007). The ubiquitous presence of mountain ranges along strike-slip faults indicates that slip partitioning is a long-term process; however, directly quantifying slip partitioning on the 10^6–10^7 years time scale is challenging because transient geometric instabilities along strike-slip faults may limit master fault strand longevity (e.g. restraining bend abandonment; Cooke et al., 2013; Wakabayashi et al., 2004), and plate convergence vectors may vary through time (Sharp & Clague, 2006).

One approach to address these challenges is to identify multiple piercing points of similar age distributed along the length of faults. Detailed geochronology, geochemistry and mapping of dismembered magmatic bodies and/or sedimentary basins can provide robust strike-slip piercing points (Fasulo et al., 2020; Leloup et al., 2013; Pundir et al., 2020). However, the correlation of dismembered magmatic bodies across faults is complicated by a growing body of research demonstrating that granitoid plutons are constructed incrementally, heterogeneous at all scales and derived from multiple end member lithospheric reservoirs (Annen, 2011; Bartley et al., 2018; Szymanowski et al., 2020). Although the role of strike-slip fault systems during pluton emplacement is disputed (Patterson & Schmidt, 1999), the linkage between strike-slip faults and volcanic

vent location is well documented (Gómez-Vasconcelos et al., 2020; Mathieu et al., 2011; Tibaldi et al., 2009). Given that volcanoes have an associated intrusive-plutonic reservoir(s), there is a clear association of magmas with arc-parallel strike-slip systems (Webb et al., 2020). Furthermore, because syn-motion pluton emplacement on the 10^6 years time scale can result in composite plutons emplaced over 10s of kms along strike on both sides of a fault system, it should be expected that dismembered plutons along strike-slip faults have overlapping age and chemistry with intra-pluton age and chemistry variability (Abbas et al., 2018; Pe-Piper et al., 1996). Understanding and documenting such variability is key to identifying dismembered plutons that may serve as reliable piercing points to reconstruct strike-slip motion.

The Denali fault system is a long-lived (>100 My; Trop et al., 2020) and active dextral fault system responsible for the highest topography in North America (Burkett et al., 2016). Late Pleistocene-Holocene slip rates along the Denali fault in Alaska decrease from east (12.9 mm/year) to west (5.3 mm/year; Figure 1; Haeussler et al., 2017) with partitioned strain accommodated in part via thrust fault splays on both sides of the fault (Bemis et al., 2015; Waldien et al., 2018, 2021). It currently accommodates ~20% of the active convergence between the Yakutat plate and North America (Elliott & Freymueller, 2020), has experienced at least 400 km of total slip since 57 Ma (e.g. Riccio et al., 2014), and delineates the boundary between the allochthonous Wrangellia Composite Terrane and rocks with a North American affinity along much of its strike length (Fitzgerald et al., 2014; Trop et al., 2019). The presence of a regionally unique suite of Eo-Oligocene plutons associated with the Denali fault zone provides a target for potential offset-marker pairs (Wilson et al., 2015). Moreover, given the high rock uplift rates leading to deep Neogene exhumation along both sides of the Denali fault (e.g. Waldien et al., 2020), it is practical to assume there are no buried Eo-Oligocene plutons proximal to the fault system that may be the actual hidden dismembered half.

Here, we leverage these well-established attributes to evaluate the stability of distributed slip partitioning on the 10^7 years time scale along this continental strike-slip fault by presenting two new Eo-Oligocene piercing points that span 500 km strike-length of the western and eastern Denali fault. These piercing points are supported by

Significance Statement

New data demonstrate that strain partitioning has been a long-term process along the Denali fault since at least ~33 Ma, suggests long-term stability of the master strand of the Denali fault system, validates a growing number of models invoking significant (>1,000 km) margin-parallel terrane translation, and represents a paradigm-shifting study with broad implications for the northern Cordillera. Most importantly, our overall study documents how obliquity may influence strike slip fault behavior and geometric stability globally and in the geologic past.

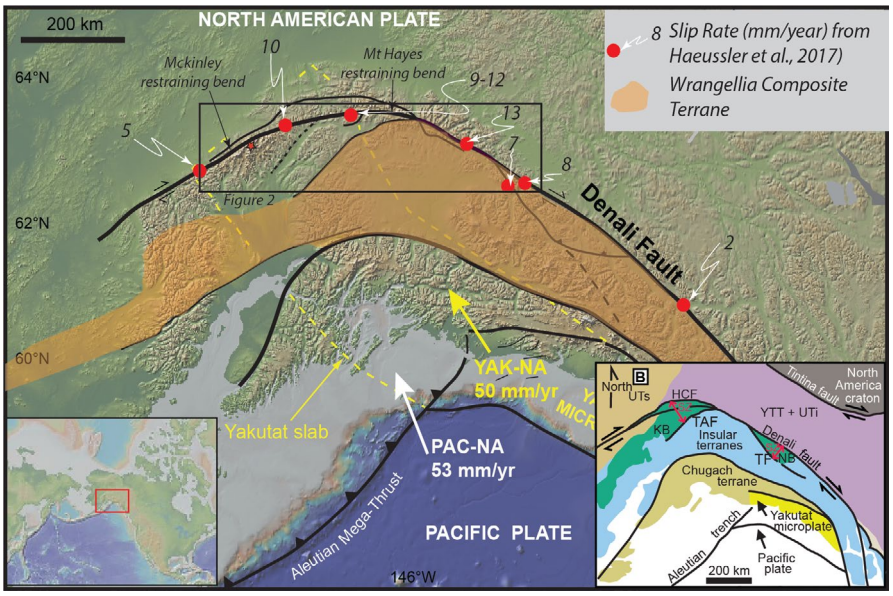

FIGURE 1 Simplified tectonic map of southern Alaska on a shaded relief base map labeled with Pleistocene-modern constraints on slip rate from Haeussler et al. (2017; *and references therein*). Dotted white line outlines the constrained distribution of the shallowly subducted Yakutat microplate. Thick white arrows show plate vectors relative to North America. Please notice that from East to West, obliquity predominant plate motion increases. Inset "B" on lower right shows Cretaceous suture zone separating Insular terranes from inboard terranes. Abbreviations: HCF, Hines Creek fault; KB, Kahiltna basin; SZ, Alaska Range Suture zone; TAF, Talkeetna fault; TF, Totschunda fault; UTi, undifferentiated terranes and igneous rocks; UTs, unidentified terranes and sedimentary rocks; YTT, Yukon-Tanana terrane [Colour figure can be viewed at wileyonlinelibrary.com]

detrital zircon U-Pb geochronology from bedrock metasedimentary samples and modern sediments sourcing isolated catchments, U-Pb zircon geochronology of igneous bedrock samples, zircon Hf isotopic tracer analysis, major and trace element geochemistry, and petrography (Tables S1–S3; the data that supports the findings of this study are available in the Supporting Information of this article).

2 | WESTERN DENALI FAULT: EOCENE PLUTONS

Late Eocene plutonic rocks are spatially associated with the Denali Fault (Wilson et al., 2015). A previous reconstruction of the late Eocene Foraker and McGonagall plutons (Figure 2) as a separated pluton across the western Denali fault, indicating a mere 38 km of displacement in 38 Ma (Reed & Lanphere, 1974), was recently disproven using paired U-Pb-Hf isotopic analysis of zircon and bulk rock major and trace element geochemistry (Figures 3 and 4; Regan et al., 2020). Here, we apply the same approach to other late Eocene plutons spatially associated with the trace of the modern Denali fault with the goal of identifying a new piercing point to constrain long-term slip rates of the western Denali fault.

We investigated if the late Eocene Panorama, Schist Creek and Nenana plutons, which are located to the north of and truncated by the Denali fault, might correlate with the Foraker pluton (Brewer, 1977; Figure 2). Based on our field observations and analytical results we interpret the Panorama, Schist Creek and Nenana plutons as the roof of a composite body separated by septa of Cretaceous strata (Cantwell Formation; Ridgway et al., 2002). The rocks of the composite Panorama-Schist Creek-Nenana pluton are K-feldspar, quartz, plagioclase, biotite granite to granodiorite and have remarkably similar major and trace element chemistry to the Foraker pluton (Figure 3; Figures S1 and S2; Table S1). U-Pb geochronology from eight samples of the composite Panorama-Schist Creek-Nenana pluton along a 50 km-long fault-parallel transect yield crystallization ages consistently younging east to west ranging from 38.46 ± 0.17 Ma (MSWD: 1.2) to 36.54 ± 0.59 (MSWD: 1.8), and εHf(t) values from approximately +6 to +12 (Figure 4; Figure S2; Table S2). The Foraker and Panorama-Schist Creek-Nenana plutons appear to be composite plutons, displaying intra-pluton variation in their geochemistry and emplacement ages (Figures 3 and 4). One sample from the Schist Creek pluton and one sample from the Foraker pluton yielded nearly identical U-Pb-Hf results of 37.82 ± 0.30 (MSWD: 1.50) and 37.59 ± 0.18 (MSWD: 0.89) and εHf(t) values from +7 to +12 and +9 to +12 respectively (Figure 4b).

The Panorama-Schist Creek-Nenana pluton and Foraker composite plutons are demonstrably similar in their age and Hf-isotope characteristics (Figure 4). Both systems are young from east to west and have consistent internal major and trace element variability. The Nenana and Foraker Plutons intrude Kahiltna formation and McKinley Sequence granite along their eastern margins. Furthermore, the overall geometry of the Panorama-Schist Creek-Nenana and Foraker composite plutons appear to be mirrored asymmetrically about the Denali fault (~50 km length; Figure 2), and we propose the entire Foraker-Panorama-Schist Creek-Nenana pluton as a new piercing point. Based on reconstructing samples with the greatest age and isotopic likeness as well as using the intersection of each pluton with McKinley Sequence granitoids and Kahiltna assemblage host rocks indicates ~155 km of slip on the Denali fault since ca. 37 Ma (Figure 4).

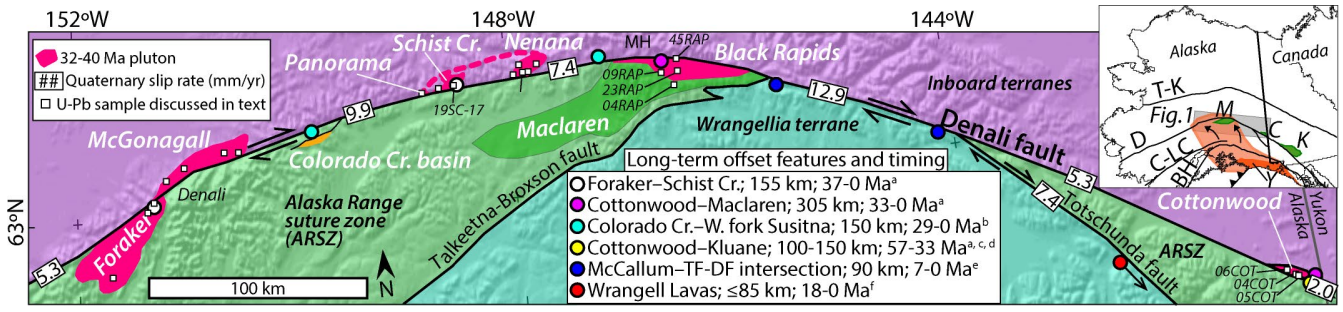

FIGURE 2 Hillshade and simplified terrane map of the central and eastern Alaska Range showing the distribution of Eo-Oligocene plutons (pink polygons) and samples discussed in text (white boxes) relative to the Denali fault and adjacent terranes. The inset location map of mainland Alaska and adjacent Canada contains major Cordilleran dextral slip faults; (T-K–Tintina-Kaltag; D-Denali; C-LC–Castle Mountain-Lake Clark; BH- Border Ranges-Hanagita). The estimated >400 km of total Cenozoic slip on the Denali fault comes from correlation of the Kluane and Maclaren terranes (K, M respectively–green polygons). Oblique convergence across the Alaska Range (depicted as bent arrows) is driven by highly coupled subduction of the Yakutat microplate (Y-orange polygon) beneath the southern Alaska margin (subducted extent depicted as light orange polygon-from Wech [2016]). Inset table contains estimates of long-term slip (colored circles) in the Denali fault system. Offset sources: a-this study; b-Nokleberg and Richter (2007); c-Nokleberg et al. (1985); d-Waldien et al., 2018; e-Berkelhammer et al. (2019). Circles with arrows indicate that the correlative rocks are not on the map. Boxed numbers along the Denali and Totschunda faults indicate the average geologic Pleistocene-Holocene slip rates (in mm/year) from Haeussler et al. (2017) [Colour figure can be viewed at wileyonlinelibrary.com]

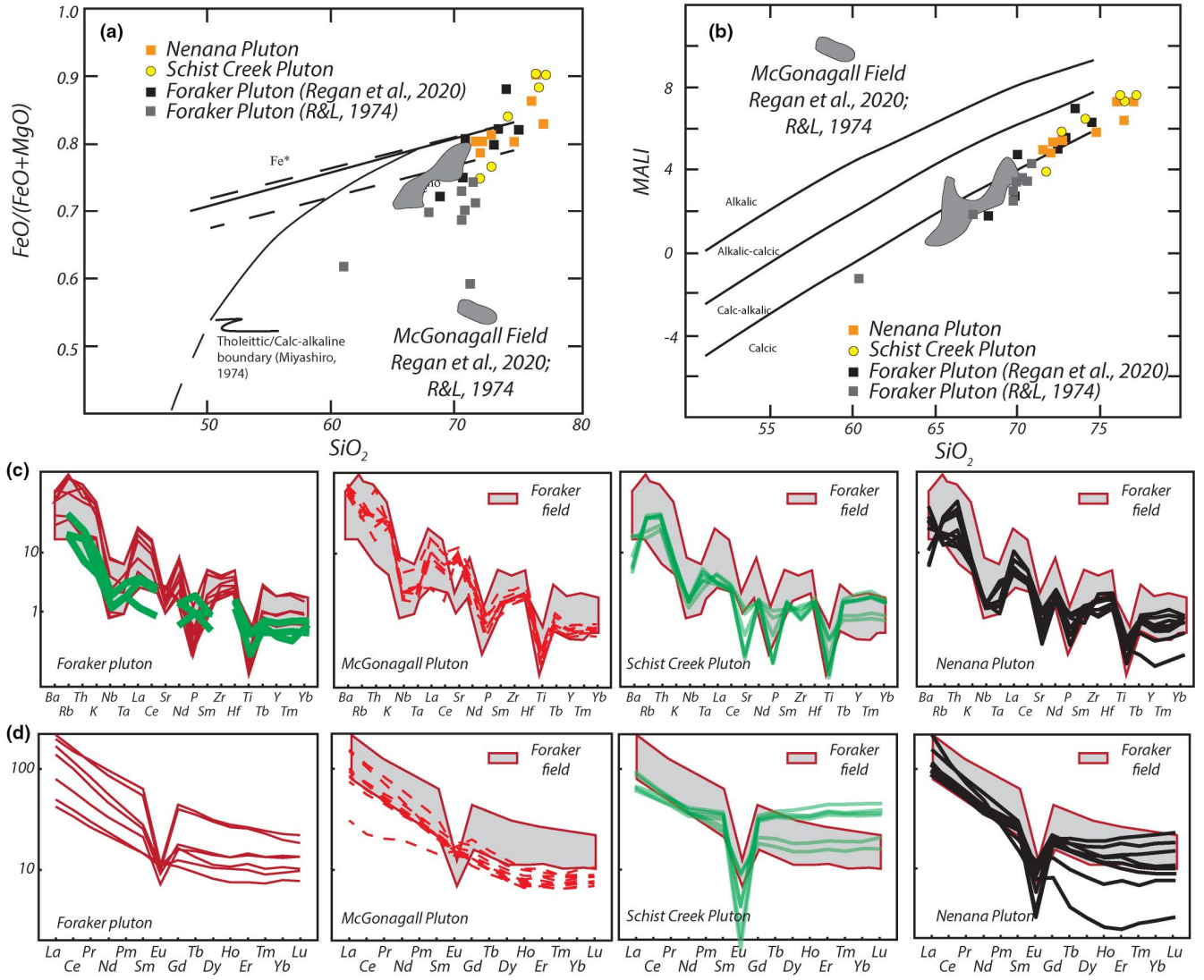

FIGURE 3 Geochemical results from the Panorama-Schist Creek-Nenana pluton compared to the Foraker and McGonagall Plutons along the Denali fault (Figures S1 and S2; Table S1). (a) Fe-index plot after Frost and Frost (2008); (b) Modified-alkali-lime-index plot (MALI) after Frost and Frost (2008); (c) Incompatible element spider diagram normalized to mid ocean ridge basalts (Gale et al., 2013) comparing data from the Foraker pluton to all other Eocene plutonic rocks analysed in this study. (d) Chondrite-normalized REE element diagram (Sun & McDonough, 1989) comparing data from the Foraker pluton to all other Eocene plutonic rocks analysed in this study. These data show much more similarities between rocks of the Foraker pluton with those from the Panorama-Schist Creek-Nenana plutons than the McGonagall pluton [Colour figure can be viewed at wileyonlinelibrary.com]

3 | EASTERN DENALI FAULT: COTTONWOOD-MACLAREN CONNECTION

Nokleberg and Richter (2007) first proposed a link between the Maclaren (south of the Denali fault) and the sliver (10 kms by 2 kms) Cottonwood (north of the Denali fault) terranes on the basis of petrographic similarity of metagranite and schist in the two terranes. Accordingly, they suggested that the two terranes represent a once coherent body that was split by the Denali fault (Figure 2). The Maclaren-Cottonwood correlation provides an opportunity to segment both the time (57 Ma to present) and >400 km distance of the oft-cited Maclaren Terrane and the Kluane Terrane (northeast of the Denali fault in Yukon) piercing point (Nokleberg et al., 1985; Riccio et al., 2014; Figure 2).

We present several lines of evidence that substantiate the correlation of Nokleberg and Richter (2007). Quantitative comparison of detrital zircon geochronologic data from schists of the Maclaren Terrane (04RAP) and the Cottonwood Terrane (05COT) indicate that the Maclaren and Cottonwood schists are more similar to each other than any of the other sedimentary successions proximal to the Denali fault (Figure 5). Multi-dimensional scaling based on cross-correlation of probability density distributions

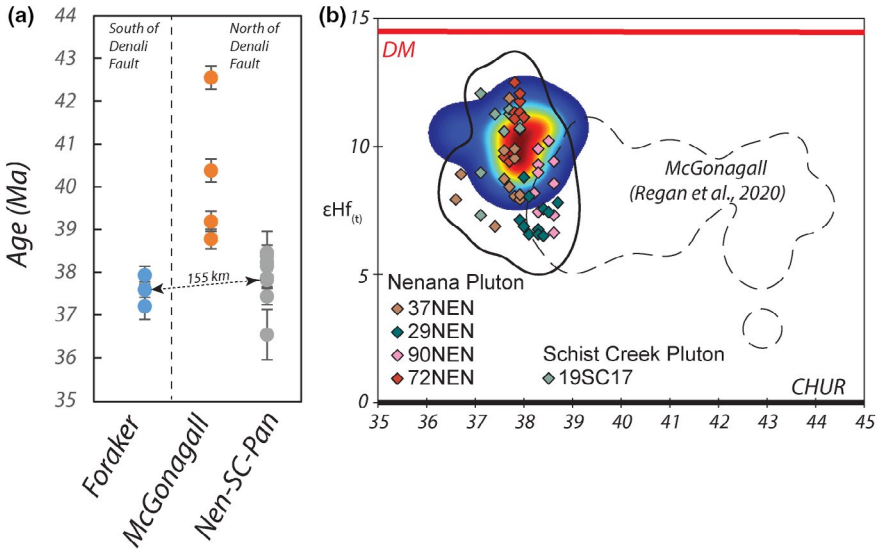

FIGURE 4 U-Pb age and Hf isotopic data from Eocene plutonic rocks from this study (Figures S1 and S2; Table S2) and Regan et al. (2020) highlighting similarities between Foraker contoured and Panorama-Schist Creek-Nenana Plutons relative to the McGonagall Pluton (Reed & Lanphere, 1974). (a) U-Pb results from all three plutonic systems; (b) $\varepsilon Hf_{(t)}$ data from all Eocene plutonic rocks displayed as bivariate kernel density estimates (KDE, Sundell et al., 2019). The dashed line indicates a 95% contour of $\varepsilon Hf_{(t)}$ data from the McGonagall pluton, and the contoured heatmap indicates $\varepsilon Hf_{(t)}$ data from the Foraker pluton (Regan et al., 2020). New data from the Panorama-Schist Creek-Nenana pluton are color coded and each diamond represents an individual zircon from which we have U-Pb and Hf-isotope data. The solid black line is the 95% contour of all new samples expressed as a combined KDE [Colour figure can be viewed at wileyonlinelibrary.com]

(Saylor & Sundell, 2016) demonstrates that Jura-Cretaceous basins along the Denali Fault form distinct groups readily distinguishable from the Cottonwood and Maclaren terranes, and support the Maclaren and Cottonwood Terranes as a unique match (Figure 5).

Several late Cretaceous and Cenozoic plutons intrude the Maclaren schist, some of which are of Eo-Oligocene in age (Figures 1 and 6; Figures S3 and S4; Table S2). Schist sample 04RAP provided two metamorphic zircon grains of Oligocene age (34.46 ± 1.66 and 35.88 ± 1.95 Ma; Figure 6). The ~23 Ma (igneous zircon U-Pb age) orthogneiss of the Cottonwood Terrane also contains a population of inherited zircon grains yielding a $^{206}Pb/^{235}U$ weighted average of 33 Ma. Interpreted to reflect the same event, one representing anatexis and the other metamorphism, our new data suggests that Maclaren and Cottonwood terranes were a coherent body until at least 33 Ma (Figure 6; Figures S3 and S4; Table S2). Bedrock plutonic (20 samples, Figures. S3 and S4; Table S2) and modern river detrital zircon U-Pb data (eight rivers, Figure 7; Figure S5; Table S2) demonstrate there are no Eocene nor Oligocene plutons exposed along the Denali fault between the Maclaren and Cottonwood Terranes, adding support to the presence of a unique piercing point match between these two now distal terranes (Figure S6). The sum of these U-Pb data establishes that the Maclaren-Cottonwood metamorphic terrane was a coherent body until at least 33 Ma when the adjoined terranes experienced ~33 Ma plutonism and have since been dismembered and translated~305 km by the Denali fault.

4 | IMPLICATIONS OF LONG-TERM SLIP PARTITIONING ALONG THE DENALI FAULT

The two new piercing points proposed herein constrain the time-averaged slip rates along the western and eastern Denali fault since ca. 33 Ma. The analytical uncertainty of our long-term slip rate calculations is minimal (<0.1 mm/year) being based on the ~1% error of the age constraints, hence no uncertainty is applied. The geochemical and isotopic similarity between the Foraker and Schist Creek-Nenana Plutons suggest ~155 km of right-lateral displacement since crystallization (ca. 37 Ma). This age-offset pair yields a time-averaged slip rate of 4.2 mm/year, similar to the 5.3 mm/year Pleistocene-Holocene slip rate for the western Denali fault defined by offset glacial features and rivers as well as exposure age dating (Haeussler et al., 2017). The Maclaren-Cottonwood Terrane correlation establishes ~305 km of displacement on the eastern Denali fault since ca. 33 Ma. This age-offset pair results in a time and along strike averaged slip rate of ~9.2 mm/year, which falls within the known range of Pleistocene-Holocene slip rate point measurements of 7.1–12.9 mm/year for this western fault segment (Haeussler et al., 2017). Consequently, the ratio of Pleistocene-Holocene slip rate between the eastern and western Denali fault is 0.41 and the new slip constraints yield a long- term (≤33 My) ratio of 0.46 (Table 1). The new data, when compiled with existing slip constraints (Figure 1), point to long-term stability of the east-to-west slip rate decrease wherein the eastern Denali fault has experienced substantially higher average

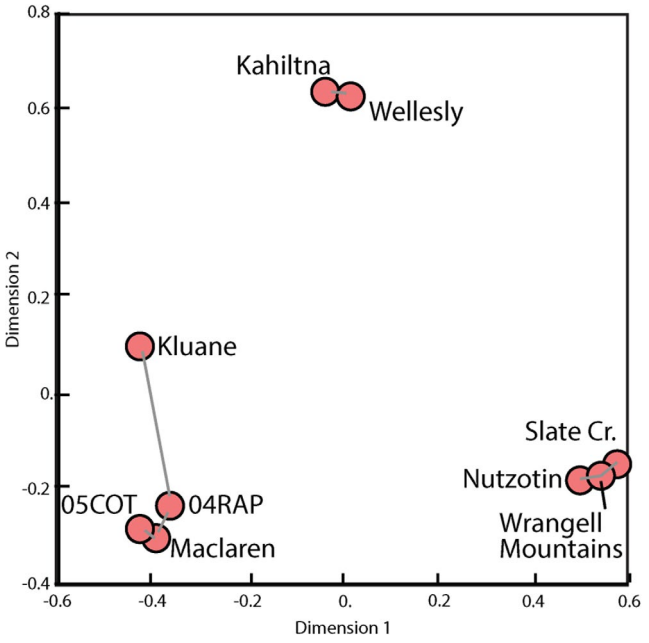

FIGURE 5 Multidimensional scaling plot based on the cross-correlation of probability density functions of the Maclaren, Kluane and Cottonwood samples relative to other Jura-Cretaceous (meta)sedimentary rocks exposed along the Denali fault. Data sources: 04RAP and 05COT-this study (Figures S2 and S3; Table S2), Maclaren-Waldien et al. (2020), Kluane-Israel et al. (2010), Wellesly, Slate Creek, Nutzotin and Wrangell Mountains-Fasulo et al. (2020), Kahiltna-Fasulo et al. (2020) and Romero et al. (2020). Plot was made using DZmds (Saylor et al., 2017). A table of the cross-correlation values from which this plot was derived is included in the data repository. Maclaren samples are more distal from the Denali fault than 04RAP and 05COT, hence experienced a slightly different metamorphic history than these two Denali fault proximal samples [Colour figure can be viewed at wileyonlinelibrary.com]

slip rates for the last ca. 33 Ma relative to the western Denali fault (Figure 8). This finding is consistent with nearly constant exhumation rates in the Mount Hayes restraining bend region since ca. 25 Ma (Benowitz et al., 2019, 2014) associated with the accommodation of partitioned strain by vertical tectonics. We infer the slightly greater amount of strain partitioning along the Denali fault documented for the Pleistocene-Holocene span compared to Oligocene-Present rate is related in part to a change in Pacific Plate convergence angle to more orthogonal (Doubrovine & Tarduno, 2008) and the development of the Mount McKinley restraining bend at ~6 Ma (Figure 1; Burkett et al., 2016).

The obliquity of convergence plays a first-order control on the evolution of slip partitioning in strike-slip fault systems. Given that the azimuth of the Denali fault trace varies by more than 50 degrees along our study region and two Pacific-North American plate vector changes have occurred in the last 25 Myr (e.g. Doubrovine & Tarduno, 2008; Jicha et al., 2018), calculating long-term convergence vectors across the Denali fault is problematic. However, geodetic data show that the Yakutat block converges with southern Alaska at a rate of ~50 mm/year along a vector of N23°W and southern Alaska moves along a similar trajectory at a significantly reduced rate relative to stable North America north of the Denali fault (Elliot et al., 2010; Figure 1). Plate circuit reconstructions suggest that southern Alaska plate deformation has involved a component of oblique convergence since the Oligocene (e.g. Jicha et al., 2018), with a theoretical Denali fault normal rate of up to 3 mm/year (Bemis et al., 2015). Furthermore, the obliquity of the Denali fault relative to the incoming plates increases to the west and is linked to a decrease in Pleistocene-Holocene slip-rates (Haeussler et al., 2017) and an increase in thrust earthquakes adjacent to the master strand (Vallage et al., 2014). Hence, the modern and ancient Denali fault

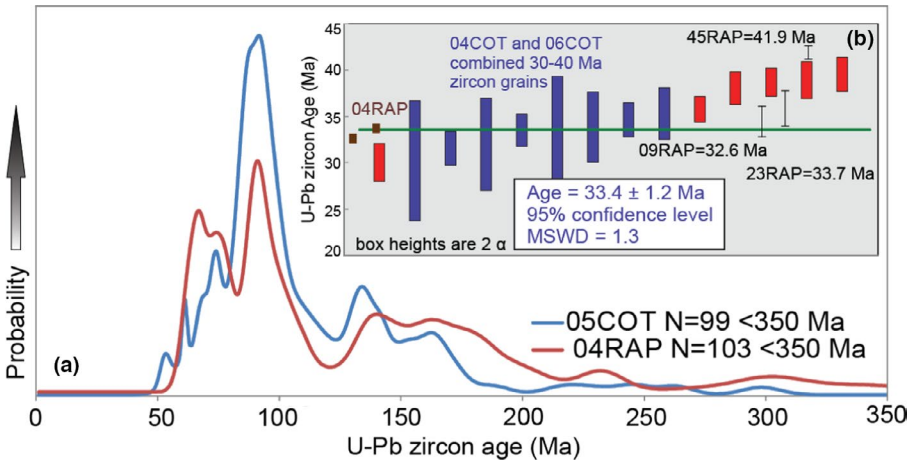

FIGURE 6 Probability density plot of detrital U-Pb zircon geochronology results from bedrock metasedimentary schists from the Cottonwood and Maclaren terranes (Figure 1; Figures S2 and S3; Table S2). Inset diagram displays post depositional U-Pb results from ortho- and paragneisses Maclaren terrane samples as well as xenocrysts from younger (ca. 23 Ma) pluton samples in the Cottonwood terrane collected 0.5 kms from each other showing consistent evidence for zircon disturbance at ca. 33 Ma. Samples 09RAP and 23RAP were collected 4 kms from each other [Colour figure can be viewed at wileyonlinelibrary.com]

system is like many highly oblique strike-slip fault systems where greater slip partitioning is linked to increased obliquity (e.g. King et al., 2005).

Despite these similarities, the Denali fault is unlike a class of strike-slip fault systems, which generally exhibit transient geometries and multiple strands (i.e. San Andreas, Marlborough

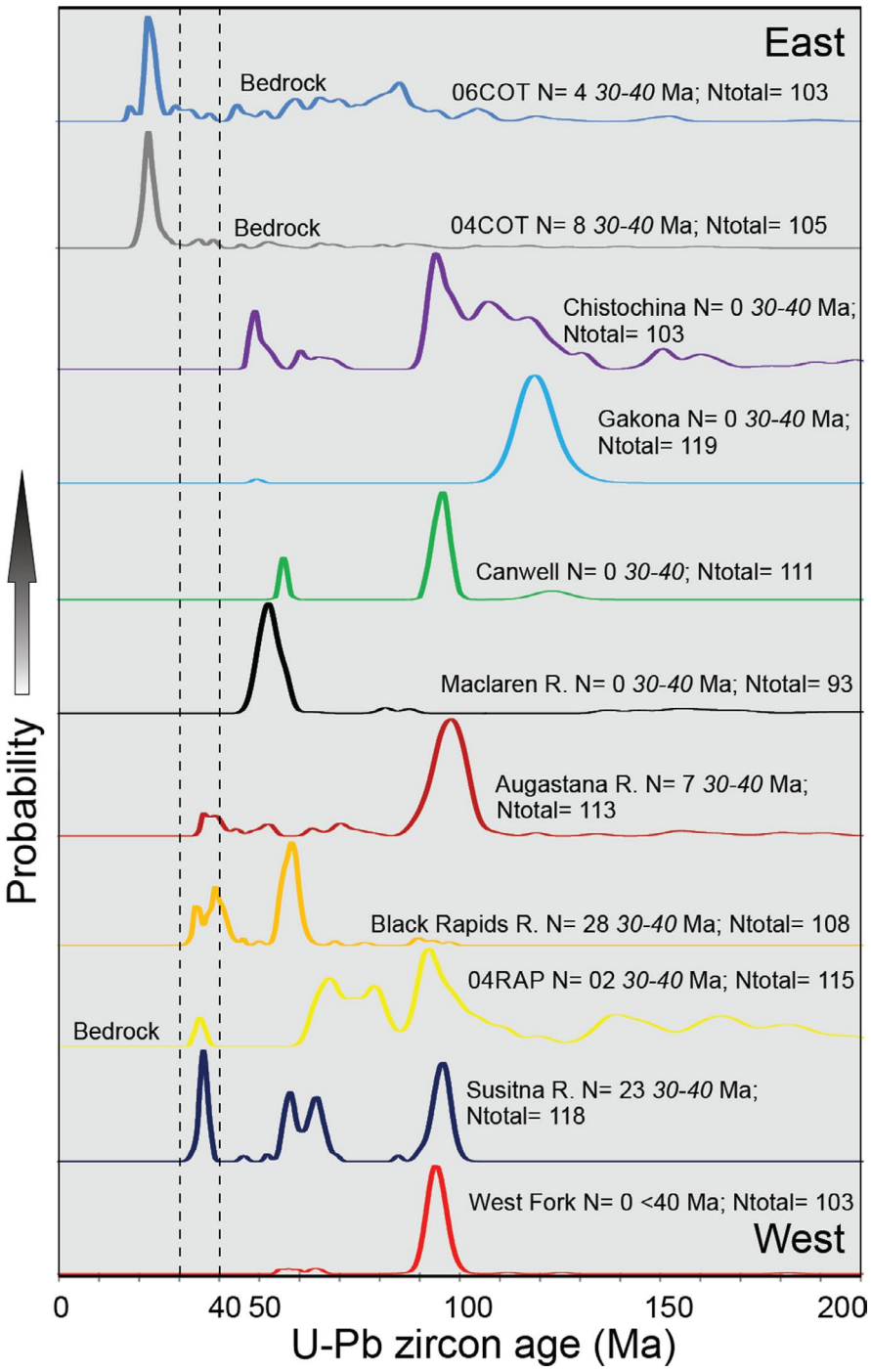

FIGURE 7 Probability density plots of U-Pb zircon single grain ages from modern river sediment samples and bedrock samples 04COT, 06COT and 04RAP demonstrating the lack of 30–40 Ma zircon sources between the Cottonwood and Maclaren Terrane (watersheds on Figure S5; Table S2) [Colour figure can be viewed at wileyonlinelibrary.com]

TABLE 1 Slip rate ratio calculations

Fault segment	Pleistocene/Holocene (mm/year)	Long-term separation (km)	Age of piercing point (Ma)	Eocene-modern slip rate (mm/year) = (separation/age)
Western Denali fault	5.3 ± 0.6	155.0	37.0	4.2
Eastern Denali fault	12.9 ± 1.5	305.0	33.0	9.2
Ratio	**0.41** (max 0.52, min 0.33)			**0.46**

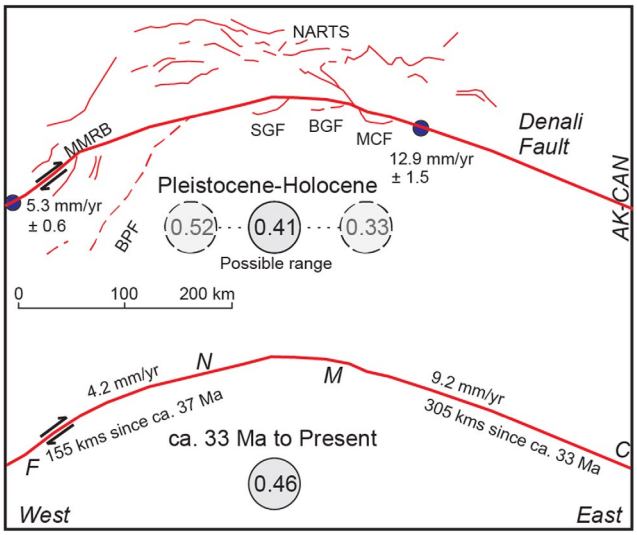

FIGURE 8 Schematic of the arcuate Denali Fault. It is a long-standing question if the great bend of the Cretaceous Denali fault bend is a feature younger than the fault and related to oroclinal bending (Hauessler et al., 2017). The ratio of slip rate decrease east to west along the Denali fault (Grey circles) is time invariable regardless of overall changes in slip rates, hence the Denali fault has been bent since at least ca. 33 Ma. Active faults shown in red (Koehler et al., 2012). The Mt McKinley restraining bend formed at ca. 6 Ma (Terhune et al., 2019) and is removed from the ca. 33 Ma to present schematic to demonstrate its influence on taking up slip. When all the thrusts and splays of the Denali fault system initiated is not known so they are not shown on the ca. 33 Ma to present schematic, but likely many of the same structures were active during this time period. (SGF—active at ca. 15 Ma—Riccio et al., 2014; MCF—active at ca. 6 Ma, Waldien et al., 2018; BGF—active at ca. 30 Ma, Waldien et al., 2021). Figure modified from Haeussler et al. (2017). Abbreviations AK-CAN, Alaska-Canada border; F, Foraker composite pluton; N, Nenana composite pluton; M, Maclaren terrane; C, Cottonwood terrane; BPF, Broad Pass thrust fault; SGF, Susitna Glacier fault; BGF, Broxson Gulch thrust fault; MCF, McCallum Creek thrust fault; NARTS, Northern Alaska Range thrust system (includes all thrusts north of the Denali fault) [Colour figure can be viewed at wileyonlinelibrary.com]

and Dead Sea fault systems). The Denali fault master strand is a narrow structure (<1 km wide) at the surface that has continuously accommodated right-lateral slip since ca. 57 Ma (Figure 1) and partitioned strain along a generally stable arcuate geometry since at least 33 Ma (this study). Other highly slip partitioned strike-slip fault systems with relatively high obliquity, (exs. Altyn Tagh, Castle Mountain, Karakorum and Kunlun fault systems) are also associated with anomalously high topography, have relatively stable (>10 Ma) master fault strands and locally extreme exhumation rates. Although lithospheric strength contrasts (Molnar & Dayem, 2010), maturity of the fault (Dolan & Haravitch, 2014) and thermal weakening due to magmatism (Garibaldi et al., 2016) factor into fault localization, we interpret the geometric stability of the Denali fault master strand relative to wrench-dominated strike-slip systems as a consequence of high obliquity. In addition to the factors mentioned above, higher obliquity promotes significant vertical tectonics, perhaps serving to localize and preserve strike-slip on the master strand between reverse fault splays.

ACKNOWLEDGEMENTS

This project was partially supported by NSF EAR #1249885 and #1828023 to Dr. Benowitz, NSF EAR #0952834 and #1828737 to Dr. Roeske, NSF EAR #2120831 to Dr. Regan, and the University of Alaska Fairbanks. Analytical support from Mark Pecha, Dominique Geisler, and the rest of the ALC crew is acknowledged. Data reduction and analysis assistance from Kurt Sundell was invaluable. Jalen Cox and Sean Mable are acknowledged for help with sample and data acquisition. The manuscript has benefited from detailed comments from Laurent Jolivet and an anonymous reviewer, which significantly improved the manuscript.

ORCID

Sean P. Regan https://orcid.org/0000-0002-8445-5138

REFERENCES

Abbas, H., Michail, M., Cifelli, F., Mattei, M., Gianolla, P., Lustrino, M., & Carminati, E. (2018). Emplacement modes of the Ladinian plutonic rocks of the Dolomites: Insights from anisotropy of magnetic susceptibility. *Journal of Structural Geology*, *113*, 42–61. https://doi.org/10.1016/j.jsg.2018.05.012

Alchalbi, A., Daoud, M., Gomez, F., McClusky, S., Reilinger, R., Romeyeh, M. A., Alsouod, A., Yassminh, R., Ballani, B., Darawcheh, R., Sbeinati, R., Radwan, Y., Masri, R. A., Bayerly, M., Ghazzi, R. A., & Barazangi, M. (2010). Crustal deformation in northwestern Arabia from GPS measurements in Syria: Slow slip rate along the northern Dead Sea Fault. *Geophysical Journal International*, *180*, 25–35. https://doi.org/10.1111/j.1365-246X.2009.04431.x

Annen, C. (2011). Implications of incremental emplacement of magma bodies for magma differentiation, thermal aureole dimensions and plutonism-volcanism relationships. *Tectonophysics*, *500*, 3–10. https://doi.org/10.1016/j.tecto.2009.04.010

Bartley, J. M., Glazner, A. F., & Coleman, D. S. (2018). Dike intrusion and deformation during growth of the Half Dome pluton, Yosemite National Park, California. *Geosphere*, *14*, 1283–1297. https://doi.org/10.1130/GES01458.1

Bemis, S. P., Weldon, R. J., & Carver, G. A. (2015). Slip partitioning along a continuously curved fault: Quaternary geologic controls on Denali fault system slip partitioning, growth of the Alaska Range, and the tectonics of south-central Alaska. *Lithosphere*, *7*, 235–246. https://doi.org/10.1130/L352.1

Benowitz, J. A., Davis, K., & Roeske, S. (2019). A river runs through it both ways across time: 40Ar/39Ar detrital and bedrock muscovite geochronology constraints on the Neogene paleodrainage history of the Nenana River system, Alaska Range. *Geosphere*, *15*, 682–701. https://doi.org/10.1130/GES01673.1

Benowitz, J. A., Layer, P. W., Armstrong, P., Perry, S. E., Haeussler, P. J., Fitzgerald, P. G., & VanLaningham, S. (2011). Spatial variations in focused exhumation along a continental-scale strike-slip fault: The Denali fault of the eastern Alaska Range. *Geosphere*, *7*, 455–467. https://doi.org/10.1130/GES00589.1

Benowitz, J. A., Layer, P. W., & Vanlaningham, S. (2014). *Persistent long-term (c. 24 Ma) exhumation in the Eastern Alaska Range constrained by stacked thermochronology*. Geological Society, Special Publications. https://doi.org/10.1144/SP378.12

Berkelhammer, S. E., Brueseke, M. E., Benowitz, J. A., Trop, J. M., Davis, K., Layer, P. W., & Weber, M. (2019). Geochemical and geochronological records of tectonic changes along a flat-slab arc transform junction: Circa 30 Ma to ca. 19 Ma Sonya Creek volcanic field, Wrangell Arc, Alaska. *Geosphere*, *15*, 1508–1538. https://doi.org/10.1130/GES02114.1

Brewer, W. M. (1977). Possibly offset plutons along the Denali fault (McKinley strand). Central Alaska Range:University of Wisconsin-Madison, MSc thesis, 261 p.

Burkett, C. A., Bernis, S. P., & Benowitz, J. A. (2016). Along-fault migration of the Mount McKinley restraining bend of Denali fault defined by late Quaternary fault patterns and seismicity, Denali National Park and Preserve, Alaska. *Tectonophysics*, *693*, 489–506.

Cooke, M. L., Schottenfield, M. T., & Buchanan, S. W. (2013). Evolution of fault efficiency at restraining bends within wet kaolin analog experiments. *Journal of Structural Geology*, *51*, 180–192. https://doi.org/10.1016/j.jsg.2013.01.010

Dolan, J. F., & Haravitch, B. D. (2014). How well do surface slip measurements track slip at depth in large strike-slip earthquakes? The importance of fault structural maturity in controlling on-fault slip versus off-fault surface deformation. *Earth and Planetary Science Letters*, *388*, 38–47. https://doi.org/10.1016/j.epsl.2013.11.043

Doubrovine, P. V., & Tarduno, J. A. (2008). A revised kinematic model for the relative motion between Pacific oceanic plates and North America since the Late Cretaceous. *Journal of Geophysical Research*, *113*, B12101. https://doi.org/10.1029/2008JB005585

Duvall, A. R., Clark, M. K., Kirby, E., Farley, K. A., Craddock, W. H., Li, C., & Yuan, D. Y. (2013). Low-temperature thermochronometry along the Kunlun and Haiyuan Faults, NE Tibetan Plateau: Evidence for kinematic change during late-stage orogenesis. *Tectonics*, *32*, 1190–1211. https://doi.org/10.1002/tect.20072

Elliot, J. L., Larsen, C. F., Freymueller, J. T., & Motyka, R. J. (2010). Tectonic block motion and glacial isostatic adjustment in southeast Alaska and adjacent Canada constrained by GPS measurements. *Journal of Geophysical Research*, *115*, B09407. https://doi.org/10.1029/2009JB007139

Elliott, J., & Freymueller, J. T. (2020). A block model of present-day kinematics of Alaska and Western Canada. *Journal of Geophysical Research: Solid Earth*, *125*. https://doi.org/10.1029/2019JB018378

Fasulo, C. R., Ridgway, K. D., & Trop, J. M. (2020). Detrital zircon geochronology and Hf isotope geochemistry of Mesozoic sedimentary basins in south-central Alaska: Insights into regional sediment transport, basin development, and tectonics along the NW Cordilleran margin. *Geosphere*, *16*, 1125–1152. https://doi.org/10.1130/GES02221.1

Fitzgerald, P. G., Roeske, S. M., Benowitz, J. A., Riccio, S. J., Perry, S. E., & Armstrong, P. A. (2014). Alternating asymmetric topography of the Alaska Range along the strike-slip Denali fault: Strain partitioning and lithospheric control across a terrane suture zone. *Tectonics*, *33*, 1519–1533. https://doi.org/10.1002/2013TC003432

Frost, B. R., & Frost, C. D. (2008). A geochemical classification for feldspathic igneous rocks. *Journal of Petrology*, *49*, 1955–1969. https://doi.org/10.1093/petrology/egn054

Gale, A., Dalton, C., Langmuir, C. H., Su, Y., & Schilling, J.-G. (2013). The mean composition of ocean ridge basalts. *Geochemistry, Geophysics, Geosystems*, *14*, 489–518. https://doi.org/10.1029/2012GC004334

Garibaldi, N., Tikoff, B., & Hernandez, W. (2016). Neotectonic deformation within an extensional stepover in El Salvador magmatic arc, Central America: Implication for the interaction of arc magmatism and deformation. *Tectonophysics*, *693*, 327–339. https://doi.org/10.1016/j.tecto.2016.05.015

Gómez-Vasconcelos, M. G., Luis Macías, J., Avellán, D. R., Sosa-Ceballos, G., Garduño-Monroy, V. H., Cisneros-Máximo, G., Layer, P. W., Benowitz, J., López-Loera, H., López, F. M., & Perton, M. (2020). The control of preexisting faults on the distribution, morphology, and volume of monogenetic volcanism in the Michoacán-Guanajuato Volcanic Field. *Geological Society of America Bulletin*, *132*, 2455–2474. https://doi.org/10.1130/B35397.1

Haeussler, P. J., Matmon, A., Schwartz, D. P., & Seitz, G. G. (2017). Neotectonics of interior Alaska and the late Quaternary slip rate along the Denali fault system. *Geosphere*, *13*, 1445–1463. https://doi.org/10.1130/GES01447.1

Israel, S., Murphy, D., Bennett, V., Mortensen, J., & Crowley, J. (2010). New insights into the geology and mineral potential of the Coast Belt in southwestern Yukon. *Yukon Exploration and Geology*, 101–123.

Jicha, B. R., Garcia, M. O., & Wessel, P. (2018). Mid Cenezoic Pacific plate motion change: Implications for the Northwest Hawaiian Ridge and circum-Pacific. *Geology*, *46*, 939–942.

King, G., Klinger, Y., Bowman, D., & Tapponnier, P. (2005). Slip-Partitioned surface breaks for the M_w 7.8 2001 Kokoxili Earthquake, China. *Bulletin of the Seismological Society of America*, *95*, 731–738. https://doi.org/10.1785/0120040101

Kirby, E., Harkins, N., Wang, E., Shi, X., Fan, C., & Burbank, D. (2007). Slip rate gradients along the eastern Kunlun fault. *Tectonics*, *26*. https://doi.org/10.1029/2006TC002033

Koehler, R. D., Farrell, R. E., Burns, P. A. C., & Combellick, R. A. (2012). *Quaternary faults and folds in Alaska: A digital database*. United States Geological Survey, Miscellaneous Investigation Map, 141, scale 1:3 700 000.

Leloup, P. H., Weinberg, R. F., Mukherjee, B. K., Tapponnier, P., Lacassin, R., Boutonnet, E., Chevalier, M. L., Valli, F., Li, H., Arnaud, N., Paquette, J.-L. (2013). Comment on "Displacement along the Karakoram fault, NW Himalaya, estimated from LA-ICP-MS U–Pb dating of offset geologic markers" published by Shifeng Wang et al in EPSL, 2012. *Earth and Planetary Science Letters*, *363*, 242–245. https://doi.org/10.1016/j.epsl.2012.12.012

Liu, J., Ren, Z., Zheng, W., Min, W., Li, Z., & Zheng, G. (2020). Late Quaternary slip rate of the Aksay segment and its rapidly decreasing gradient along the Altyn Tagh fault. *Geosphere*, *16*(6), 1538–1557. https://doi.org/10.1130/GES02250.1

Mahmoud, Y., Masson, F., Meghraoui, M., Cakir, Z., Alchalbi, A., Yavasoglu, H., Yönlü, O., Daoud, M., Ergintav, S., & Inan, S. (2013). Kinematic study at the junction of the East Anatolian fault and the Dead Sea fault from GPS measurements. *Journal of Geodynamics*, *67*, 30–39. https://doi.org/10.1016/j.jog.2012.05.006

Mathieu, L., van Wyk de Vries, B., Pilato, M., & Troll, V. R. (2011). The interaction between volcanoes and strike-slip transtensional and transpressional fault zones: Analogue models and natural examples. *Journal of Structural Geology*, *33*, 898–906. https://doi.org/10.1016/j.jsg.2011.03.003

Matmon, A., Schwartz, D. P., Haeussler, P. J., Finkel, R., Lienkaemper, J. J., Stenner, H. D., & Dawson, T. E. (2006). Denali fault slip rates and Holocene–late Pleistocene kinematics of central Alaska. *Geology*, *34*, 645–648. https://doi.org/10.1130/G22361.1

Miyashiro, A. (1974). Volcanic rock series in island arcs and active continental margins. *American Journal of Science*, *274*, 321–355. https://doi.org/10.2475/ajs.274.4.321

Molnar, P., & Dayem, K. E. (2010). Major intracontinental strike-slip faults and contrasts in lithospheric strength. *Geosphere*, *6*, 444–467. https://doi.org/10.1130/GES00519.1

Nokleberg, W. J., Jones, D. L., & Silberling, N. J. (1985). Origin and tectonic evolution of the Maclaren and Wrangellia terranes, eastern Alaska Range, Alaska. *Geological Society of America Bulletin*, *96*, 1251–1270. https://doi.org/10.1130/0016-7606(1985)96<1251:OATEOT>2.0.CO;2

Nokleberg, W. J., & Richter, D. H. (2007). Origin of narrow terranes and adjacent major terranes occurring along the Denali fault in the Eastern and Central Alaska Range, Alaska. *Special Papers-Geological Society of America*, *431*, 129.

Norris, R. J., & Cooper, A. F. (2001). Late Quaternary slip rates and slip partitioning on the Alpine Fault, New Zealand. *Journal of Structural Geology*, *23*, 507–520. https://doi.org/10.1016/S0191-8141(00)00122-X

Patterson, S. R., & Schmidt, K. L. (1999). Is there a close relationship between faults and plutons. *Journal of Structural Geology*, *21*, 1131–1142.

Pe-Piper, G., Piper, D. J., & Koukouvelas, I. (1996). Precambrian plutons of the Cobequid Highlands, Nova Scotia, Canada. *Special Papers-Geological Society of America*, 121–132.

Pundir, S., Adlakha, V., Kumar, S., Singhal, S., & Sen, K. (2020). Petrology, geochemistry and geochronology of granites and granite gneisses in the SE Karakoram, India: Record of subduction-related and pre-to syn-kinematic magmatism in the Karakoram Fault Zone. *Mineralogy and Petrology*, *114*, 413–434. https://doi.org/10.1007/s00710-020-00706-y

Reed, B. L., & Lanphere, M. A. (1974). Offset plutons and history of movement along the McKinley segment of the Denali fault system, Alaska. *Geological Society of America Bulletin*, *85*, 18831892. https://doi.org/10.1130/0016-7606(1974)85<1883:OPAHOM>2.0.CO;2

Regan, S. P., Benowitz, J. A., & Holland, M. E. (2020). A plutonic brother from another magma mother: Disproving the Eocene Foraker-McGonagall pluton piercing point and implications for long term slip on the Denali fault. *Terra Nova*, *32*, 66–74. https://doi.org/10.1111/ter.12437

Riccio, S. J., Fitzgerald, P. G., Benowitz, J. A., & Roeske, S. M. (2014). The role of thrust faulting in the formation of the eastern Alaska Range: Thermochronological constraints from the Susitna Glacier thrust fault region of the intracontinental strike-slip Denali fault system. *Tectonics*, *33*, 2195–2217. https://doi.org/10.1002/2014TC003646

Ridgway, K. D., Trop, J. M., Nokleberg, W. J., Davidson, C. M., & Eastham, K. R. (2002). Mesozoic and Cenozoic tectonics of the eastern and central Alaska Range: Progressive basin development and deformation in a suture zone. *Geological Society of America Bulletin*, *114*, 1480–1504. https://doi.org/10.1130/0016-7606(2002)114<1480:MACTOT>2.0.CO;2

Romero, M. C., Ridgway, K. D., & Gehrels, G. E. (2020). Geology, U-Pb geochronology, and Hf isotope geochemistry across the Mesozoic Alaska Range suture zone (south-central Alaska): Implications for Cordilleran collisional processes and tectonic growth of North America. *Tectonics*, *39*, e2019TC005946. https://doi.org/10.1029/2019TC005946

Saylor, J. E., Jordan, J. C., Sundell, K. E., Wang, X., Wang, S., & Deng, T. (2017). Topographic growth of the Jishi Shan and its impact on basin and hydrology evolution, NE Tibetan Plateau. *Basin Research*, *30*, 544–563. https://doi.org/10.1111/bre.12264

Saylor, J. E., & Sundell, K. E. (2016). Quantifying comparison of large detrital geochronology data sets. *Geosphere*, *12*, 203–220. https://doi.org/10.1130/GES01237.1

Sharp, W. D., & Clague, D. A. (2006). 50-Ma initiation of Hawaiian-Emperor bend records major change in Pacific plate motion. *Science*, *313*, 1281–1284. https://doi.org/10.1126/science.1128489

Spotila, J. A., House, M. A., Niemi, N. A., Brady, R. C., Oskin, M., Buscher, J. T., Till, A. B., Roeske, S. M., Sample, J. C., & Foster, D. A. (2007). Patterns of bedrock uplift along the San Andreas fault and implicatios for mechanisms of transpression. *Special Papers-Geological Society of America*, *434*, 15–33.

Sun, S.-S., & McDonough, W. F. (1989). Chemical and isotopic systematics of oceanic basalts: Implications for mantle composition and processes. *Geological Society of London Special Publications*, *42*, 313–345. https://doi.org/10.1144/GSL.SP.1989.042.01.19

Sundell, K. E., Saylor, J. E., & Pecha, M. (2019). Sediment provenance and recycling of detrital zircons from Cenozoic Altiplano strata in southern Peru and implications for the crustal evolution of west-central South America. In B. K. Horton & A. Folguera (Eds.), *Andean Tectonics*, (pp. 363–397). Elsevier.

Szymanowski, D., Forni, F., Wolff, J. A., & Ellis, B. S. (2020). Modulation of zircon solubility by crystal-melt dynamics. *Geology*, *48*, 798–802. https://doi.org/10.1130/G47405.1

Tatar, O., Poyraz, F., Gürsoy, H., Cakir, Z., Ergintav, S., Akpınar, Z., Koçbulut, F., Sezen, F., Türk, T., Hastaoğlu, K. Ö., Polat, A., Mesci, B. L., Gürsoy, Ö., Ayazlı, İ. E., Çakmak, R., Belgen, A., & Yavaşoğlu, H. (2012). Crustal deformation and kinematics of the Eastern Part of the North Anatolian Fault Zone (Turkey) from GPS measurements. *Tectonophysics*, *518*, 55–62. https://doi.org/10.1016/j.tecto.2011.11.010

Terhune, P. J., Benowitz, J. A., Trop, J. M., O'Sullivan, P. B., Gillis, R. J., & Freymueller, J. T. (2019). Cenozoic tectono-thermal history of the southern Talkeetna Mountains, Alaska: Insights into a potentially alternating convergent and transform plate margin. *Geosphere*, *15*(5), 1539–1576. https://doi.org/10.1130/GES02008.1

Tibaldi, A., Pasquare, F., & Tormey, D. (2009). Volcanism in reverse and strike-slip fault settings. In S. Cloetingh & J. Negendank (Eds.), *New Frontiers in Integrated Solid Earth Science*, (pp. 315–348). Springer. https://doi.org/10.1007/978-90-481-2737-5_9

Trop, J. M., Benowitz, J. A., Cole, R., & O'Sullivan, P. (2019). Cretaceous to Miocene magmatism, sedimentation, and exhumation within the Alaska Range suture zone: A reactivated terrane boundary. *Geosphere*, *16*, 1066–1101.

Trop, J. M., Benowitz, J. A., Koepp, D. O., Sunderlin, D., Bueseke, M. E., Layer, P. W., & Fitzgerald, P. G. (2020). Stitch in the ditch: Nutzotin Mountains (Alaska) fluvial strata and a dike record ca. 117–114 Ma accretion of Wrnngellia with western North America and initiation of the Totschunda fault. *Geosphere*, *16*, 82–110.

Vallage, A., Deves, M. H., Klinger, Y., King, G. C. P., & Ruppert, N. A. (2014). Localized slip and distributed deformation in oblique settings: The example of the Denali fault system, Alaska. *Geophysical Journal International*, *197*, 1284–1298. https://doi.org/10.1093/gji/ggu100

Wakabayashi, J., Hengesh, J. V., & Sawyer, T. L. (2004). Four-dimensional transform fault processes: Progressive evolution of step-overs and bends. *Tectonophysics*, *392*, 279–301. https://doi.org/10.1016/j.tecto.2004.04.013

Waldien, T. S., Roeske, S. M., Benowitz, J. A., Allen, W. K., Ridgway, K. D., & O'Sullivan, P. B. (2018). Late miocene to quaternary evolution of the Mccallum Creek thrust system, Alaska: Insights for range-boundary thrusts in transpressional orogens. *Geosphere*, *14*, 2379–2406. https://doi.org/10.1130/GES01676.1

Waldien, T. S., Roeske, S. M., Benowitz, J. A., Twelker, E., & Miller, M. S. (2020). *Oligocene-Neogene lithospheric-scale reactivation of Mesozoic terrane accretionary structures in the Alaska Range suture zone, southern Alaska*. GSA Bulletin.

Waldien, T. S., Roeske, S. M., & Benowitz, J. A. (2021) (in press). Tectonic underplating and dismemberment of the Maclaren-Kluane schist records late Cretaceous terrane accretion polarity and ~480 km of post-52 Ma dextral displacement on the Denali fault: Accepted to Tectonics.

Webb, M., White, L. T., Jost, B. M., Tiranda, H., & BouDagher-Fadel, M. (2020). The history of Cenozoic magmatism and collision in NW New Guinea-New insights into the tectonic evolution of the northernmost margin of the Australian Plate. *Gondwana Research*, *82*, 12–38. https://doi.org/10.1016/j.gr.2019.12.010

Wech, A. G. (2016). Extending Alaska's plate boundary: Tectonic tremor generated by Yakutat subduction. *Geology*, *44*(7), 587–590.

Wilson, F. H., Hults, C. P., Mull, C. G., & Karl, S. M. (2015). *Geologic map of Alaska: U.S. Geological Survey Scientific Investigations Map 3340*, 196 p., scale 1:1,584,000, https://doi.org/10.3133/sim3340

Zeng, Y., & Shen, Z. K. (2014). Fault network modeling of crustal deformation in California constrained using GPS and geologic observations. *Tectonophysics*, *612*, 1–17. https://doi.org/10.1016/j.tecto.2013.11.030

Zheng, W. J., Zhang, P. Z., He, W. G., Yuan, D. Y., Shao, Y. X., Zheng, D. W., Ge, W. P., & Min, W. (2013). Transformation of displacement between strike-slip and crustal shortening in the northern margin of the Tibetan Plateau: Evidence from decadal GPS measurements and late Quaternary slip rates on faults. *Tectonophysics*, *584*, 267–280. https://doi.org/10.1016/j.tecto.2012.01.006

SUPPORTING INFORMATION

Additional Supporting Information may be found online in the Supporting Information section.

Figure S1. Central Alaska range map

Figure S2. Eastern Alaska range map

Figure S3. Cottonwood area map

Figure S4. 30-40 Ma U-Pb zircon single grain ages from the Cottonwood and Maclaren Terrane piercing point rocks (Figure 1) demonstrating the overlap of this discrete Alaska Range age population

Figure S5. Watershed map of modern river sediment samples

Figure S6. New and existing detrital zircon geochronology from along the Denali Fault (modified after Fasulo et al. (2020)). Data sources: 04RAP and 05COT- this study (Figs. DR2 and DR3; Table DR2), Maclaren-Waldien et al. (2020), Kluane- Israel et al. (2011), Wellesly, Slate Creek, Nutzotin, and Wrangell Mountains- Fasulo et al. (2020), Kahiltna- Fasulo et al. (2020) and Romero et al. (2020).

Table S1. Whole rock major and trace element geochemistry of plutonic rocks along the Denali Fault.

Table S2. Sampling locations and descriptions for U-Pb samples.

Table S3. A to Z analytical methods.

How to cite this article: Regan, S. P., Benowitz, J. A., Waldien, T. S., Holland, M. E., Roeske, S. M., O'Sullivan, P., & Layer, P. (2021). Long distance plutonic relationships demonstrate 33 million years of strain partitioning along the Denali fault. *Terra Nova*, 33, 630–640. https://doi.org/10.1111/ter.12555